HHS Public Access

Author manuscript

Nat Methods. Author manuscript; available in PMC 2012 June 01.

Published in final edited form as:

Nat Methods. ; 8(12): 1027–1036. doi:10.1038/nmeth.1768.

Evaluation of fluorophores for optimal performance in localization-based super-resolution imaging

Graham T. Dempsey[1,6], **Joshua C. Vaughan**[2,3,6], **Kok Hao Chen**[3,6], **Mark Bates**[4], and **Xiaowei Zhuang**[2,3,5,*]

[1]Graduate program in Biophysics, Harvard University, Cambridge, MA 02138

[2]Howard Hughes Medical Institute, Harvard University, Cambridge, MA 02138

[3]Department of Chemistry and Chemical Biology, Harvard University, Cambridge, MA 02138

[4]School of Engineering and Applied Sciences, Harvard University, Cambridge, MA 02138

[5]Department of Physics, Harvard University, Cambridge, MA 02138

Abstract

One approach to super-resolution fluorescence imaging uses sequential activation and localization of individual fluorophores to achieve high spatial resolution. Essential to this technique is the choice of fluorescent probes — the properties of the probes, including photons per switching event, on/off duty cycle, photostability, and number of switching cycles, largely dictate the quality of super-resolution images. While many probes have been reported, a systematic characterization of the properties of these probes and their impact on super-resolution image quality has been described in only a few cases. Here, we quantitatively characterized the switching properties of 26 organic dyes and directly related these properties to the quality of super-resolution images. This analysis provides a set of guidelines for characterization of super-resolution probes and a resource for selecting probes based on performance. Our evaluation identified several photoswitchable dyes with good to excellent performance in four independent spectral ranges, with which we demonstrated low crosstalk, four-color super-resolution imaging.

INTRODUCTION

The spatial resolution limit of light microscopy imposed by diffraction has recently been overcome by super-resolution fluorescence imaging methods[1,2]. Among these methods, stochastic optical reconstruction microscopy (STORM)[3] and (fluorescence) photoactivated

*To whom correspondence should be addressed. zhuang@chemistry.harvard.edu.

6These authors contributed equally to this work.

AUTHOR CONTRIBUTIONS

G.T.D., J.C.V., K.H.C., and X.Z. designed the experiments. G.T.D., J.C.V., K.H.C., and M.B. performed the experiments. G.T.D., J.C.V., and K.H.C. performed the data analysis and interpretation. G.T.D., J.C.V., and X.Z. wrote the manuscript. X.Z. supervised the project.

COMPETING FINANCIAL INTERESTS

The authors declare no competing financial interests.

localization microscopy ((F)PALM)[4,5] achieve sub-diffraction-limit resolution by sequentially imaging and localizing individual fluorophores that label the target structure. The basic concept of single-molecule-localization-based super-resolution imaging entails: (i) sparse activation of an optically resolvable subset of fluorophores, (ii) determination of the positions of these fluorophores with sub-diffraction-limit accuracy, and (iii) repeating this process to allow stochastically different subsets of fluorophores to be turned on and localized each time (Fig. 1a). An image with sub-diffraction-limit resolution can then be reconstructed from the positions of the numerous activated molecules.

As stated in the original STORM paper[3], "we demonstrate the concept of STORM using the cyanine switch, but in principle any suitable optically switched fluorophore could be used" and "the STORM concept is also applicable to other photoswitchable fluorophores and fluorescent proteins". Indeed, a variety of fluorescent probes have been utilized for localization-based super-resolution imaging, including organic dyes[3,6–21], fluorescent proteins[4,5,22,23], and quantum dots[24]. In the simplest imaging mode, continuous illumination of a single dye (e.g., Alexa 647) with a single laser wavelength can generate high-quality STORM images, where the laser accomplishes all three tasks of activating the dye to the fluorescent state, exciting fluorescence from the dye, and switching it off to the dark state[14]. Like Alexa 647, a variety of commonly used organic dyes spanning a broad spectrum of colors can transition between fluorescent and dark states and have been used for super-resolution imaging[8,10,11,14–16]. Depending on the fluorescent probes used, this imaging method has also been referred to by several other acronyms (e.g., dSTORM[11,15]), which use the same fundamental imaging principle as STORM -- a technique generally applicable to photoswitchable probes.

A key factor affecting the quality of STORM images is the choice of switchable probes. The photoswitchable probes can be largely divided into two categories (Fig. 1b): (i) reversibly switchable probes that can be converted between fluorescent (on) and dark (off) states multiple times upon excitation by light either of the same or different wavelengths, and (ii) irreversibly activatable probes that exist initially in a dark state and can be activated by light to a fluorescent state. Examples in the first category include photoswitchable cyanine, rhodamine, and oxazine dyes[3,6,7,10,15,16] and photoswitchable fluorescent proteins such as Dronpa[25], Dreiklang[26], and rsEGFP[27]. Examples in the second category include dark-to-bright fluorescent proteins, such as PA-GFP[28] and PA-mCherry[29], color-converting fluorescent proteins, such as PS-CFP[30], EosFP[31,32], and Dendra2[33], and push-pull fluorogen dyes[18], although in some cases photoactivatable fluorescent proteins may also undergo reversible photoswitching once photoactivated. In addition to photoswitchable fluorophores, probes that can be turned on and off by non-optical means, such as reversible ligand binding[34] or by fluorescent quenchers[19], have also been used for localization-based super-resolution fluorescence microscopy (Fig. 1b).

Here we focused on reversibly photoswitchable dyes, which include the majority of organic dyes used for localization-based super-resolution imaging. Two properties of switchable probes crucial to super-resolution image quality are: (i) the number of photons detected per switching event, and (ii) the on/off duty cycle (or the fraction of time a fluorophore spends in the on state)[2,35]. Switching events with a high photon yield are desired for accurate

determination of a probe's position due to the inverse-square-root dependence of the localization precision on the number of detected photons[36,37]. Hence the photon number limits the obtainable optical resolution. A low duty cycle is generally beneficial since the maximum number of fluorophores that can be localized within a diffraction-limited area is inversely proportional to the duty cycle (a fluorophore with a duty cycle of 1/N typically allows less than N molecules to be localized within a diffraction-limited area). This maximum fluorophore density in turn limits the image resolution according to the Nyquist sampling criterion[38], which equates the maximal achievable resolution to twice the average distance between neighboring probes. The importance of the number of photons per switching event and the duty cycle are illustrated in Figure 2a–c for three hypothetical cases: (i) A fluorophore with a high photon yield per switching event and a low duty cycle provides both high localization precision and high localization density, and is thus able to resolve small structures, such as a hollow ring in this case (Fig. 2a); (ii) A fluorophore with a low photon yield can only be localized with low precision and consequently blurs out the hollowness of the ring structure (Fig. 2b); (iii) A fluorophore with a high on/off duty cycle limits the density of probes that can be localized within a diffraction-limited area, which also obscures the hollow ring structure due to an insufficient number of localizations (Fig. 2c).

Although many fluorophores have been utilized for STORM, relatively few have been quantitatively and systematically characterized in terms of photon yield and on/off duty cycle, let alone other important properties that influence image quality or acquisition speed, such as the photostability, the total number of photoswitching cycles, and the ability to control the fluorophore activation rate by a light source independent from the imaging light. Furthermore, the imaging buffer conditions can strongly impact the fluorophore switching properties and the resulting image quality[12,39], and yet the roles of different buffer components are not well understood for many fluorophores. Consequently, the incomplete quantitative information on the photoswitching properties makes it difficult for practitioners to systematically choose the optimal fluorophores and imaging conditions for attaining high quality super-resolution images.

In this Analysis article, we addressed this problem by evaluating 26 commercially available fluorophores and their suitability for STORM imaging. We focused on organic dyes that can reversibly switch between on and off states before photobleaching. We provided single-molecule characterization of the number of photons detected per switching event, the on/off duty cycle, the photostability, and the sensitivity to photoactivation by violet light for all dyes, and corroborated these measurements with STORM images in all cases to demonstrate the impact of a dye's switching properties on image quality. We also explored the importance of buffer conditions on dye performance. Our characterization provides a resource of quantitative information about each fluorophore's switching properties to facilitate fluorophore selection for STORM applications, as well as a set of guidelines for evaluating the fitness of fluorophores for STORM in general. We also identified several high-quality switchable dyes in different spectral ranges, which we used to demonstrate low-crosstalk, four-color super-resolution imaging.

RESULTS

We evaluated 26 organic dyes spanning the visible and near infrared (NIR) spectral range. These dyes include: blue-absorbing (Atto 488, Alexa 488, Atto 520, fluorescein, FITC, Cy2), yellow-absorbing (Cy3B, Alexa 568, TAMRA, Cy3, Cy3.5, Atto 565), red-absorbing (Alexa 647, Cy5, Atto 647, Atto 647N, Dyomics 654, Atto 655, Atto 680, Cy5.5), and NIR-absorbing (DyLight 750, Cy7, Alexa 750, Atto 740, Alexa 790, IRDye 800CW) fluorophores. They can be categorized structurally as cyanines (Cy2, Cy3, Cy3B, Cy3.5, Cy5, Alexa 647, Dyomics 654, Cy5.5, Cy7, DyLight 750, Alexa 750, Alexa 790, IRDye 800CW), rhodamines (Alexa 488, Atto 488, Atto 520, TAMRA, Atto 565, Alexa 568), oxazines (Atto 655, Atto 680), carbopyronines (Atto 647N, Atto 647, Atto 740), and fluoresceins (FITC, fluorescein).

Previously, STORM imaging has been performed either with activator-reporter dye pairs[3,6,12,14,40,41], in which "activator" molecules are used to enhance the activation rate of the photoswitchable "reporter" molecules, or photoswitchable reporters alone[8,10,11,14–16]. Since the intrinsic properties of the photoswitchable reporters limit the STORM imaging performance in both cases in a similar manner, we characterized these properties in the reporter-alone configuration.

Method of photoswitchable probe characterization

We characterized the switching properties using dye-labeled proteins that were adsorbed to coverglass and illuminated with light at 488 nm, 561 nm, 647 nm, or 752 nm, to excite blue, yellow, red, or NIR dyes, respectively. Under these conditions, many fluorophores reversibly transition between on and off states with a characteristic duty cycle and number of emitted photons per switching event. Although it is often convenient to use an additional “activation laser” to increase the on-switching rate and hence speed up the imaging process, the on/off duty cycle determined in the absence of the activation laser represents the lowest achievable duty cycle for a dye and thus sets the resolution limit based on the Nyquist criterion. The number of detected photons per switching event is typically the same independent of whether an additional activation light is used.

For each dye, we determined four switching properties: (i) number of photons detected per switching event; (ii) on/off duty cycle; (iii) survival fraction; and (iv) number of switching cycles. We recorded the number of photons detected in each switching event for many molecules, from which we constructed a photon number histogram and determined the mean value. The on/off duty cycle was measured as the fraction of time spent in the on state averaged over many molecules. Because the molecules were originally in the on state and a certain illumination time is required for them to reach a quasi-equilibrium between the on and off states, we used a sliding window of 100 sec to monitor changes in the on/off duty cycle as a function of exposure time. The duty cycle value during the time window 400–600 sec was used to represent the characteristic, equilibrium duty cycle because the dyes typically achieved quasi-equilibrium between on and off states by this point. Since some dyes switched for a limited number of cycles before photobleaching, a substantial fraction of molecules may be photobleached by the time the on/off equilibrium is reached. We therefore also characterized the survival fraction of unbleached molecules as a function of

illumination time. This quantity can be used together with the time-dependent duty cycle value to determine what degree of photobleaching has occurred prior to achieving a sufficiently low density to resolve single molecules. Finally, we also determined for each molecule the number of switching cycles during the data acquisition time, which represents a lower bound value given that some molecules did not photobleach before the end of the observation period.

We correlated the above properties with the quality of STORM images for each dye by recording images of different cellular structures, including microtubules which have a linear (or cylindrical) morphology, and clathrin-coated pits (CCPs) which have a spherical morphology. Because the switching performance and photostability of many dyes are enhanced by the presence of a primary thiol and/or a low oxygen environment, we performed experiments in the presence of an enzymatic oxygen scavenging system and a primary thiol, either β-mercaptoethanol (βME) or mercaptoethylamine (MEA), unless otherwise indicated.

Figure 2d–l illustrates our method of dye characterization, using Alexa 647, Atto 655, and Cy5.5 as representative examples. We show examples of single-molecule fluorescence time traces (Fig. 2d–f, Supplementary Fig. 1), histograms of photon number distributions (Fig. 2g,i,k), and duty cycle plots along with the corresponding survival fractions (Fig. 2h,j,l). The dyes exhibited three distinct switching behaviors: high photon yield per switching event and low duty cycle (Alexa 647); low photon yield and low duty cycle (Atto 655); and high photon yield and high duty cycle (Cy5.5).

Photon number and duty cycle

To demonstrate the importance of photon number and duty cycle, we recorded three-dimensional (3D) STORM images of CCPs, which provided an excellent metric for assessing a dye's performance because of their small size (~100–200 nm diameter) and the requirement for high spatial resolution to reveal their hollow, spherical shell-like structure. The 3D STORM images were taken using astigmatism imaging, the most easily implemented 3D super-resolution imaging approach[40]. When imaging Alexa 647-labeled CCPs, the hollow shape of the pit was clearly resolved (Fig. 2m–p) due to the high photon yield of individual switching events (~5,000 photons, Fig. 2g) and low on/off duty cycle (~0.001, Fig. 2h). The *xy*- and *xz* cross-sections taken from the midplanes of an example CCP demonstrate the expected cup-like shape of the pit (Fig. 2n,o). The superposition of *xy* cross-sections of multiple CCPs showed the expected hollow, ring-like structure (Fig. 2p).

In contrast to Alexa 647, the low photon yield of Atto 655 (~660 photons per switching event, Fig. 2i), and the resulting low localization precision, blurred the CCP image substantially such that its hollowness was no longer apparent (Fig. 2q–t), despite the fact that the duty cycle of Atto 655 (~0.001, Fig. 2j) was comparable to that of Alexa 647. In a different manner, the high duty cycle of Cy5.5 (~0.007, Fig. 2l) also negatively impacted the quality of the CCP images (Fig. 2u–x). Because of the large fraction of time each dye spent in the fluorescent state, a considerable reduction in labeling density (or photobleaching of molecules prior to imaging) was necessary to ensure single-molecule detection and localization. As a result, the sparse localization pattern no longer resolved the hollow

morphology of the CCP, despite the high photon yield of Cy5.5 (~6,000 photons per switching event, Fig. 2k). These examples demonstrate that both high photon number and low duty cycle are essential to achieving high-resolution STORM images. In Supplementary Figures 2–27 and Table 1, we show the wide range of photon number and duty cycle values of the 26 dyes.

Photostability and number of switching cycles

The dyes also exhibited large variations in their survival fraction and number of switching cycles before photobleaching (Supplementary Figs. 2–27, Table 1). Although the three dyes in Figure 2 showed comparably high survival fractions after the molecules reached an on/off equilibrium state (Fig. 2h,j,l), some dyes photobleached much more rapidly. For example, Cy2 showed little recovery to the on state after the initial switching off event, and by the time the duty cycle reached equilibrium, only a very small fraction of molecules survived. Consequently, we were unable to reconstruct a STORM image using Cy2 (Supplementary Fig. 7). An interesting example is Atto 565 (Supplementary Fig. 13). Despite having the highest photon yield per switching cycle among all the dyes screened, its relatively low survival fraction upon reaching on/off equilibrium led to overall lower quality STORM images compared to many other dyes with lower photon yields but higher survival fractions.

Related to the survival fraction is the number of switching cycles afforded by a fluorophore. While it is desirable to have a single switching cycle for some applications, such as for the purpose of counting molecules, in many cases, a large number of switching events is advantageous. Specifically, the detection of multiple switching events from the same fluorophore reduces the stochasticity of the localization error, and in the limit of many cycles, the mean localization positions converge with the true positions of the fluorophores. (Supplementary Fig. 28a). This effect directly impacts the STORM image quality in that a dye with a low number of switching cycles often results in an image with more jagged and ill-defined spatial features due to localization errors, whereas a dye with a large number of switching cycles results in a smoother and more continuous image due to repetitive sampling of the same structure and thus lower noise in the final image (Supplementary Fig. 28b). For instance, dyes with relatively few switching cycles, such as Cy3, produced STORM images with sparse localization densities and overall poor quality, despite its high photon number and low on/off duty cycle (Supplementary Fig. 11). In contrast, fluorophores that exhibited a high number of switching cycles, such as Atto 488 (Supplementary Fig. 2), resulted in more continuous and better-defined microtubule or CCP structures, in spite of a relatively low photon yield.

Sensitivity of fluorophores to violet light activation

During acquisition of a STORM movie, the number of molecules present in a given frame decreases as the fluorophores are photobleached. This reduction, in turn, decreases the information content in a single frame and increases the number of frames required to construct an image. The use of an “activation” laser of a different wavelength from the excitation laser can increase the activation rate and thus reduce the image acquisition time. In the case of activator-reporter pairs, the activator molecules allow the reporter to be activated by using visible light of different colors[6]. When a photoswitchable reporter alone

is used for STORM imaging, the activation rate is typically controlled by an ultraviolet or violet light[10,20,39]. We tested how the dyes responded to short wavelength activation by switching a field of molecules to a stable dark state and then measuring the fraction of molecules that recovered following a pulse of violet (405 nm) light. Several red and NIR dyes showed appreciable recovery after 405 nm illumination, while even the most sensitive blue and yellow dyes showed modest recovery (Table 2).

Dependence of switching properties on buffer composition

The switching properties of dyes can depend strongly on buffer composition. We tested the switching performance of all dyes under four different buffer conditions: (i) our standard buffers containing both an oxygen scavenging system (glucose oxidase with catalase, or GLOX) and a primary thiol (βME or MEA) — "GLOX + thiol"; (ii) a buffer with GLOX but no thiol — "GLOX only"; (iii) a buffer with a thiol (MEA) but no GLOX — "Thiol only", and (iv) a buffer with neither GLOX nor thiol — "No GLOX or thiol". We found that nearly all of the tested dyes photobleached rapidly under the "No GLOX or thiol" or "Thiol only" conditions, while several dyes switched reasonably well in the "GLOX only" condition (Atto 488, Alexa 488, Atto 520, Cy3B, and Atto 680; see Table 3 and Supplementary Figs. 29–30). All 26 dyes achieved equal or better imaging results when using buffers containing both GLOX and thiol (Table 2, Supplementary Figs. 29–30).

To more concretely illustrate the effect of thiol or oxygen on dye switching, we quantitatively characterized the switching properties of Alexa 647, Atto 488, and Atto 655 under the four buffer conditions stated above (Supplementary Fig. 29). Consistent with previous observations, Alexa 647 required thiol for photoswitching and the photon yield per switching cycle, photostability, and number of switching cycles further increased when oxygen was removed by GLOX[42–44]. In contrast, Atto 488 switched well in the absence of thiol, but performed best in buffer containing GLOX. In particular, the photostability of Atto 488 increased in the order of “No GLOX or thiol” or "Thiol only" < "GLOX only" < "GLOX + thiol", and this order correlated well with STORM image quality. In the case of Atto 655, which has been previously proposed to switch well in the presence of a thiol under ambient (high) oxygen concentrations without the need of an oxygen scavenger system[15], we observed substantially better performance in the "GLOX + thiol" condition and found that even the "GLOX only" condition yielded better photostability and image quality than the "Thiol only" condition.

Different thiols can be used to facilitate switching of dyes. We quantitatively characterized all 26 dyes in both MEA (10 mM) and βME (140 mM), where the chosen thiol concentrations were in the range of typical usage reported previously[6,12,39]. In some cases, the switching behavior was rather sensitive to the thiol concentration, as illustrated by more detailed investigations of Atto 488, Cy3B, Alexa 647, Atto 655, and DyLight 750. We found that low to moderate concentrations of MEA enhanced the dye’s switching performance and STORM image quality (Table 3, Supplementary Fig. 29), but high concentrations (100 mM) of MEA diminished either the number of switching cycles (Cy3B), or the number of photons per switching cycle (Atto 488 and Alexa 647), or both (DyLight 750 and Atto 655) (Supplementary Fig. 31). Optimal performance was achieved under relatively low MEA

concentrations for these five dyes (1–10 mM, Supplementary Fig. 31), in contrast to the 50–200 mM concentrations previously recommended[12,39].

Some dyes also behaved differently in the presence of different thiols. For instance, the duty cycles of Atto 488 and Alexa 647 were substantially lower in the presence of MEA than in βME (Supplementary Figs. 2, 14)[12], w h ile DyLight 750 showed the opposite trend (Supplementary Fig. 22). More dramatically, STORM images of good quality could be acquired with Atto 647N and Alexa 750 in the presence of βME, whereas the survival fractions for both dyes were reduced to a nearly unusable level when using MEA (Supplementary Fig. 17, 24).

These results emphasize the importance of buffer formulation in STORM imaging. We therefore recommend that practitioners optimize buffer conditions for a given probe.

Dependence of switching properties on light intensity

The imaging laser intensity is another adjustable parameter during STORM imaging. Often, we found the number of photons per switching cycle to be largely independent of laser intensity because both the photon emission rate and off-switching rate tend to depend linearly on the excitation intensity (Supplementary Fig. 32). Some exceptions were observed, such as the case of Cy3B where the number of photons per switching cycle increased with the excitation intensity (Supplementary Fig. 32). The equilibrium duty-cycle values also did not vary substantially with the laser intensity, as expected when both off- and on-switching rates depend linearly on the excitation intensity. On the other hand, we observed a decrease in the survival fraction and the total number of switching cycles with increased excitation intensity for some dyes, such as Atto 655 (Supplementary Fig. 32). Therefore, while strong excitation intensity is often used to increase the switching rate and thus imaging speed, excessive laser intensity could reduce the image quality.

Summary of characterization for 26 dyes

Table 1 summarizes all four important properties that affect the STORM image quality, photon number, duty cycle, survival fraction, and number of switching cycles. Full details are included in Supplementary Figures 2–27 for each of the 26 fluorophores, including dye structures (when available), fluorescence excitation and emission spectra, representative single-molecule fluorescence traces, photons per switching event, duty cycle, survival fraction, as well as 2D STORM images of microtubules and CCPs. Table 2 summarizes the sensitivity of the dyes to activation by violet (405 nm) light, and Table 3 summarizes the on/off switching performance under different buffer conditions.

Overall, we observed large variability in the switching properties of the different dyes. The number of detected photons per switching event ranged from a few hundred to several thousand (Table 1). This wide range led to wide variability in the localization precision and hence STORM image resolution. An even broader range of duty cycles was observed, spanning two orders of magnitude from 0.0001 to 0.04 (Table 1). While the duty cycle can be adjusted to some extent by changing buffer conditions, in particular by the use of different thiols[12,39], for some dyes, this parameter is simply too high to obtain adequate image quality despite the broad range of conditions tested.

Accordingly, the STORM image qualities afforded by these dyes also showed large variability. Dyes with high photon numbers, low duty cycles, high survival fractions, and many switching cycles in general performed well and produced high quality images (discussed below), while dyes with low photon numbers, high duty cycles, low survival fractions, and/or few switching cycles did not (e.g., fluoresein, FITC, Cy2, Cy3, Atto 565, Cy5.5, Atto 740, Alexa 790, IRDye 800CW).

Several dyes within our screen showed good overall properties, resulting in high-quality super-resolution images. Among these dyes, Alexa 647 (along with its structural analog Cy5) and Dyomics 654 emerged as top choices for their overall excellent properties. When used to image microtubules, we observed that Alexa 647 and Dyomics 654 were able to resolve the hollowness of immunostained microtubule filaments (Fig. 3). The transverse profile of localizations (Fig. 3c–d) shows two resolved peaks separated by 36–38 nm, as expected for the projection of a 25 nm diameter cylinder that has been broadened by primary antibodies prior to staining with dye-labeled secondary antibodies.

Multi-color STORM imaging with spectrally distinct dyes

From our screen we identified dyes with good performance in each of four distinct spectral ranges (blue: 480–540 nm, yellow: 545–600 nm, red: 640–700 nm, and NIR: 740–805 nm) to demonstrate four-color STORM imaging. These dyes were Atto 488 in the blue range, Cy3B in the yellow range, Alexa 647, Cy5, and Dyomics 654 in the red range, and DyLight 750, Cy7, and Alexa 750 in the NIR range. Several of these dyes (Atto 488, Dyomics 654, DyLight 750, and Cy7) were used for STORM imaging for the first time. It should be noted that the red dyes Alexa 647, Cy5, and Dyomics 654 performed considerably better than even the best-performing dyes in other spectral regions. In comparison, Atto 488, Cy3B, DyLight 750, Cy7, and Alexa 750 were substantially dimmer, and Cy3B additionally exhibited a lower number of switching cycles and a wider distribution of photons per switching cycle. Nevertheless, when compared to other dyes within each corresponding spectral band, these dyes exhibited the best overall performance in terms of photon output, duty cycle, survival fraction, number of switching cycles, and quality of super-resolution images.

To demonstrate four-color imaging, we first imaged a model sample of *in vitro* prepared microtubules labeled with Atto 488, Cy3B, Alexa 647 (or Dyomics 654), and DyLight 750 (Fig. 4a, Supplementary Fig. 33a). The microtubules were labeled separately with each of these dyes and then mixed prior to imaging. The excellent spectral separation afforded by the probes (Fig. 4b, Supplementary Fig. 33b) allowed us to achieve low crosstalk between the four channels (Fig. 4c–f, Supplementary Fig. 33c–f). We observed 0–3% crosstalk between different channels, except for Cy3B which exhibited higher crosstalk (~8%) into the Atto 488 and Alexa 647 (or Dyomics 654) channels (Fig. 5g, Supplementary Fig. 33g). Quantitative analysis of single, repetitively switching fluorophores allowed us to determine the localization precisions to be 29 nm for Atto 488, 22 nm for Cy3B, 17 nm for Alexa 647 (or Dyomics 654), and 30 nm for DyLight 750 (measured as the full-width at half maximum of the localization distribution of individual probes, Supplementary Fig. 34). The variation corresponded well with photons per switching event for each dye.

Finally, we demonstrated the utility of these probes in multicolor imaging of four different cellular targets. For this, we immunostained cells for tubulin, Tom20 (marker for mitochondrial outer membrane), ATL1 (marker for endoplasmic reticulum (ER)), and acetylated tubulin using Atto 488, Cy3B, Alexa 647, and DyLight 750, respectively. Figure 5a–d shows STORM images for each of the four individual channels over the same field of view within a single cell. The excellent spectral separation allowed for easy color distinction of each cellular structure. Figure 5e–f shows the magnified, overlaid images of the ER with mitochondria and microtubules with acetylated tubulin, respectively. In many instances, mitochondria nestled with extensive contacts with the ER network (Fig. 5e). As expected, only a subset of microtubules are acetylated (Fig. 5f). Similar results were obtained when replacing Alexa 647 with Dyomics 654 (Supplementary Fig. 35).

DISCUSSION

Single-molecule-localization-based super-resolution imaging has been rapidly adopted by researchers for ultra-structural characterization of biological samples. The wide variation in the fluorophore properties underscores the importance of probe choice in this imaging method. The dye screen we performed provides a resource to practitioners by giving quantitative characterizations of relevant switching properties of a range of fluorescent dyes and by illustrating how these properties impact the quality of super-resolution images.

We showed that fluorophore performance can be quantified in terms of four parameters, namely the number of photons per switching event, the on/off duty cycle, the survival fraction as the dye reaches on/off equilibrium, and the number of switching cycles before photobleaching, and that these properties in large part dictate the quality of the super-resolution images (Fig. 2, Supplementary Figs. 2–27, Table 1). In general, fluorophores with high photon yield per switching event, low on/off duty cycle, high survival fraction, and large number of switching cycles are desired for producing high-quality STORM images. Additional fluorophore parameters not included in this study may also be of significance, such as heterogeneity of switching properties across molecules (e.g., variations in photon output or switching kinetics from molecule to molecule, which were appreciable for Cy3B) or compatibility with living cells. Another untested variable which may be pertinent is excitation wavelength. For example, Cy5.5 and IRDye 800CW, which showed the highest on/off duty cycles amongst all dyes tested, were evaluated using excitation wavelengths (647 nm and 752 nm, respectively) that differed substantially (by ~30 nm) from their absorption peaks. Better matching of the excitation wavelength to the absorption maximum may help to minimize the duty cycle value, as we have observed for Alexa 647 (data not shown).

The choice of buffer composition is another important factor in achieving robust on/off switching of dyes. We tested two specific buffer additives, a primary thiol and an oxygen scavenging system. For all dyes investigated, the best results were obtained with the imaging buffer containing both a primary thiol and an oxygen scavenging system. Regardless of their structures, the dyes in our screen typically performed better in the presence of an oxygen scavenging system. For some dyes (i.e. Atto 488, Alexa 488, Atto 520, Cy3B, and Atto 680), on/off switching and reasonably good STORM performance were achieved even when

thiol was omitted (Supplementary Fig. 29–30, Table 3). These observations suggest that a stable dark state could be achieved for these dyes by a thiol-independent pathway distinct from the previously suggested thiol-dependent formation of dark radical or reduced species[45]. In contrast, red and NIR-cyanine dyes, such as Alexa 647, require a thiol for robust switching (Supplementary Fig. 29), consistent with the previous finding that they form a covalent conjugate with the thiol in the dark state[44]. The concentration and identity of the thiol can also quantitatively impact the dye's switching properties and the STORM image quality (Supplementary Fig. 31). Non-thiol buffer additives such as ascorbic acid and methyl viologen can also be used to switch dyes[16], although we have not explored the use of these buffer additives here. In general, investigation of the photochemical mechanisms underlying dark state formation is challenging due to the presence of different types of dark states[10,44–47] and the fact that buffer components, such as thiol or dissolved oxygen, can play different roles (as reducing agents, triplet state quenchers, radical scavengers, etc.). Studies to elucidate physical mechanisms of photoswitching should help rational design of optimal buffer conditions.

From this screen, we identified dyes suitable for STORM within each of four separate spectral bands (blue, yellow, red, and NIR) and demonstrated four-color STORM imaging using these probes (Fig. 5,6, Supplementary Figs. 33,35). This approach of using probes with minimal spectral overlap[8] gave lower crosstalk between color channels than multi-color approaches that use probes with the same emission color but different activation wavelengths (by pairing different activators with the same reporter)[6] or that use two-channel ratiometric detection of fluorophores with partially overlapping spectra[48]. Furthermore, the low crosstalk was achieved without sacrificing the density of molecules, as occurs when detecting two or more channels that overlap spectrally. On the other hand, the use of different activation wavelengths[6] or ratiometric detection methods[48] also offers advantages over the multi-color imaging scheme used here. For instance, multiple activator-reporter pairs may be implemented using the highest performing dye (Alexa 647, or its close structural analogs), which performs far better than fluorophores in the other spectral channels, thus enabling multi-color super-resolution imaging with high resolution in all color channels[6,12,41]. Only one detection channel is required in this case, allowing automatic and perfect registration of the different color channels. Ratiometric detection of two or more spectrally overlapped fluorophores can be performed in principle with a single imaging laser and allows all fluorophores to be imaged simultaneously[48]. We note, however, that the spectrally distinct fluorophores used here may also be imaged simultaneously using multichannel detection, although the intense short wavelength light used to image blue or yellow dyes could potentially over-activate the red or NIR dyes, and care should be taken when pursuing this strategy.

Finally, it is worth noting that we have only sampled a small subset of organic dyes and imaging buffer conditions, leaving open the possibility of even better probes and more optimal imaging conditions yet to be identified. In addition to organic dyes, a systematic and comparative study of photoswitchable fluorescent proteins[23] would also be of great benefit to practitioners. The criteria we established here may be used in the future for testing probes not included in the current analysis. A thorough understanding of the important probe

properties will facilitate optimal probe selection for effective applications of super-resolution fluorescence microscopy.

METHODS

Methods and any associated references are available in the online version of the paper at http://www.nature.com/naturemethods/.

METHODS

Dyes and antibodies

Dyes were obtained from Amersham (Cy2, Cy3, Cy3B, Cy3.5, Cy5, Cy5.5, Cy7), Invitrogen (Alexa 488, Alexa 568, Alexa 647, Alexa 750, Alexa 790), ATTO-TEC (Atto 520, Atto 565, Atto 647, Atto 655, Atto 680, Atto 740), Sigma (Atto 488, Atto 647N), Anaspec (5(6)-TAMRA), Pierce (FITC, fluorescein, DyLight 750), Dyomics (Dyomics 654), and LI-COR (IRDye 800CW). All purchased dyes contained an N-hydroxysuccinimidyl ester (NHS) group for conjugation to protein, with the exception of FITC, which contains an isothiocyanate moiety for protein coupling. Primary antibodies were purchased from: Abcam (mouse anti-clathrin, ab2731; rat anti-tubulin, ab6160; mouse anti-acetylated tubulin, ab24610; goat anti-myc, ab9132), and Santa Cruz Biotechnology (rabbit anti-TOM20, sc-11415). Unconjugated secondary antibodies were purchased from Jackson ImmunoResearch Laboratories, including donkey anti-mouse (715-005-151), donkey anti-rat (712-005-153), donkey anti-rabbit (711-005- 152), and bovine anti-goat (805-005-180).

Fluorescence microscope

All single-molecule and imaging measurements were performed on an Olympus IX-71 inverted microscope configured for either total internal reflection fluorescence (TIRF) or oblique incidence excitation. In the oblique incidence geometry, the incidence angle was slightly below the critical angle such that the excitation light illuminated 1–2 μm deep into the sample in the field of view. The samples were continuously illuminated using different excitation sources depending on the fluorophore used. Blue- and red-absorbing dyes were excited using the 488 nm and 647 nm lines of a mixed-gas argon-krypton laser (Innova 70C; Coherent), respectively; yellow-absorbing dyes were excited with a 561 nm diode-pumped solidstate laser (Sapphire 561; Coherent); NIR-absorbing dyes were excited using the 752 nm line of a krypton laser (Innova 302C; Coherent). A 405 nm solid state laser (Cube 405–100C; Coherent) was used for activation of dyes as described below. Beam selection and modulation of the laser intensities were controlled in a number of ways, depending on the laser wavelength. For 488 nm and 647 nm lines, an acousto-optic tunable filter (AA Optoelectronic) was used. The 561 nm and 752 nm lines were controlled using mechanical shutters (Uniblitz). For the 405 nm line, the light was controlled by direct digital modulation of the laser power supply. In all cases, neutral density filter wheels were used for coarse adjustments of laser power along with a combination of a half-wave plate and polarizer for fine power adjustments.

The following longpass dichroic mirrors were used to reflect the excitation sources listed above: T495LP (Chroma) for 488 nm, Di01-R561 (Semrock) for 561 nm, Z660DCXRU

(Chroma) for 647 nm, and Q770DCXR (Chroma) for 752 nm. Fluorescence was collected using an Olympus UPlanSApo 100×, 1.4 NA oil immersion objective lens and passed through either one of the following bandpass emission filters: 535/50 (ET535/50m; Chroma) for blue-absorbing dyes; 617/73 (FF01-617/73-25; Semrock) for yellow-absorbing dyes; 700/75 (ET700/75m; Chroma) for red- absorbing dyes; or 800/60 (HQ800/60m; Chroma), for NIR-absorbing dyes. All movies were recorded onto a 256×256 pixel region of an electron-multiplying charge coupled device (EMCCD) camera (iXon 897; Andor).

During data acquisition, a home-built focus lock was used to maintain a constant focal plane as described previously[49]. Briefly, a 975 nm IR laser diode (PL980P330J; Thorlabs) was directed towards the sample using a dichroic mirror (900DCSP; Chroma). The beam reflected off of the sample was detected by a quadrant photodiode (QPD). Changes in the axial position of the sample resulted in a shift of the reflected beam position on the QPD. A feedback system using custom LabVIEW software then adjusted the sample z-position using a piezo stage (NZ100CE; Prior Scientific) until the original beam position was restored.

Imaging buffers

Detailed single-molecule characterization and STORM imaging for each dye (Figs. 2–5, Table 1–3, Supplementary Figs. 1–35) was performed in an imaging buffer that contained TN buffer (50 mM Tris, pH 8.0, 10 mM NaCl), an oxygen scavenging system (0.5 mg/mL glucose oxidase (G2133; Sigma-Aldrich), 40 μg/mL catalase (106810; Roche Applied Science or C100–50MG; Sigma-Aldrich), and 10% (w/v) glucose), and either 143 mM 2-hydroxy-1-ethanethiol (βME; Fluka) or 10 mM 2-aminoethanethiol (MEA; Fluka), unless otherwise indicated. MEA was stored as a solid at 4°C and prepared fresh as a 1 M stock solution in water with pH adjusted to ~8 with 1 M aqueous KOH. This stock solution was kept at 4°C and used within 1–2 weeks of preparation. βME was stored as a neat liquid (14.3 M) at 4°C. For experiments, the thiol solutions were diluted immediately before imaging to the final concentrations as described above.

Buffer dependence experiments (Supplementary Figs. 29–30, Table 3) were performed using one of the following four different buffers: PBS only (“No GLOX or thiol” condition); TN buffer with 10 mM MEA (“thiol only” condition); TN buffer with oxygen scavenger with the above described composition (“GLOX only” condition); and TN buffer with 10 mM MEA and oxygen scavenger with the above described composition (“GLOX and thiol” condition). To assess whether any free thiol was present in the “GLOX only” solution, we measured the absorption increase at ~410 nm of the “GLOX only” buffer upon addition of 50 μM Ellman’s reagent (5,5′-Dithiobis(2-nitrobenzoic acid), D8130; Sigma-Aldrich), a standard assay for free thiol quantification[50]. No absorption increase was detectable. In contrast, absorption increase was observed for a series of standard cysteine solutions with concentrations ranging between 1–20 μM. This measurement placed an upper limit of the thiol concentration of our “GLOX only” buffer to <1 μM.

Single-molecule sample preparation

Single-molecule characterization of fluorophores was performed using dye-labeled donkey anti-rat secondary antibodies. Antibodies were labeled using the manufacturers’ protocols.

In brief, 10 μL of 1 M aqueous $NaHCO_3$ pH 8.0 is added to 50–100 μg of antibody to a final antibody concentration of ~2 μM. Dyes were dissolved in dimethyl sulfoxide and added to antibody solutions at varying dye concentrations (typically at a final concentration of ~4 μM to achieve the desired dye to protein ratios). Dyes could be stored for long term as a solid at −20°C. Labeled antibodies were purified by gel filtration using Nap-5 columns (17-0853; GE Healthcare). The labeling ratio was determined using a Beckman-Coulter UV-Vis spectrophotometer. All dye-labeled antibodies for single-molecule characterization measurements had dye labeling ratios 0.2–0.8 dyes per antibody such that the majority of dye-labeled antibody molecules were labeled with only one dye molecule. Labeled antibodies were immobilized onto the surface of a flow chamber assembled from a glass slide and a #1.5 coverslip that were separated by double-sided tape. Slides and coverslips were cleaned by sonication for 15 minutes in each of the following: Alconox solution, followed by Mili-Q water, followed by 100% ethanol, and lastly 1 M aqueous potassium hydroxide. Coverslips were then washed with Mili-Q water and blow-dried with compressed nitrogen prior to assembly of the flow chamber. The labeled antibodies were adsorbed to the coverslip at a low density (typically 0.04–0.12 dye/μm^2) such that individual dye molecules could be clearly resolved from each other. Control experiments showed that labeled antibodies do not detach from the surface on the time scale of the experiments (data not shown). The flow chambers were rinsed extensively with phosphate buffered saline (PBS) to remove unbound antibodies prior to imaging.

Single-molecule fluorescence measurements

Blue-, yellow-, red-, and NIR-absorbing dyes were illuminated with 488 nm (1.2 kW/cm^2), 561 nm (2.2 kW/cm^2), 647 nm (0.8 kW/cm^2), or 752 nm (1.3 kW/cm^2) laser light in a total-internal reflection geometry. Under constant illumination and the buffer conditions described in the “Imaging buffers” section, the dyes typically started in the fluorescent state, switched to a dark state, and spontaneously recovered to a fluorescent state multiple times before photobleaching. For each dye, several movies of 1,500–2,000 sec duration were recorded, and 50–150 single-molecule fluorescence time traces were obtained per movie. All movies were collected at a frame rate of 33 Hz. Control samples lacking fluorescently labeled antibodies, but otherwise prepared in the same way, yielded virtually no detected fluorescent molecules in each of the four spectral ranges studied (data not shown). The low density of adsorbed fluorescent antibodies (<0.1/μm^2) and the low number of dyes per antibody molecule (<0.8/antibody) was chosen to minimize the probability that fluorescent signals being studied originated from more than one dye molecule. Additional control experiments were performed to assess what fraction of fluorescent signals originated from single fluorophores by imaging adsorbed dye-labeled antibodies under buffer conditions that have been previously shown to drastically reduce fluorophore blinking (TN buffer with GLOX and 1 mM Trolox)[51]. These experiments revealed that >90% of fluorescent spots showed single-step photobleaching, ensuring single-molecule detection under our imaging conditions.

Single-molecule data analysis

In the initial frame of each single-molecule characterization movie, the positions of adsorbed molecules were determined by identifying fluorescent signals above a threshold of 4 times

the standard deviation of the fluctuations of the detected background signal. Any fluorescent molecule within 5 pixels (peak to peak separation, with 160 nm per pixel) of another fluorescent molecule was omitted from analysis. Fluorescence time traces were calculated for each molecule by analyzing the total integrated signal within a 7×7 pixel region centered on the molecule during each frame of the movie. The number of photons detected per switching event was calculated as the total integrated signal minus the background intensity counts, which was converted to photons using the calibrated curve for the electron multiplication and ADC gain settings used during acquisition. Fluorescence switching events were identified within the time traces by identifying signal changes with a magnitude that is greater than 5–10 times the standard deviation of the background fluctuations of the fluorescence time trace. The on/off duty cycle, D.C., of the dyes was calculated within a sliding window of 100 sec as:

$$D.C. = \left\langle \frac{\sum_i \tau_{on,i}}{100 sec} \right\rangle$$

where $\tau_{on,i}$ denotes the on-time of the i^{th} switching event for a given molecule within the time window, and the brackets indicate averaging over all molecules not yet photobleached. The equilibrium duty cycle reported was the mean of the duty cycle value between 400–600 sec. Photobleached molecules were not included in the duty cycle calculation for times past photobleaching. Note that we only report the duty cycle and survival fraction, i.e. the fraction of dyes not yet photobleached, for the first 700 sec of illumination although the total movie was 2000 sec long. Therefore, only molecules that photobleached within the first 700 sec need to be identified. Here, we consider a molecule to be bleached after the final on event identified for that molecule in the movie. The molecules that were identified to be bleached during the first 700 sec based on this criterion most likely have in fact been photobleached given that the remaining 1300 sec of the movie is typically 4–20 times longer in duration than the mean off time of each fluorophore.

To measure dye sensitivity to activation by violet light, samples were first illuminated for 1500 frames at 20 Hz frame rate at their respective excitation wavelength (488, 561, 647, or 752 nm) to switch most dyes into a dark state. After this, the imaging laser was turned off and a 0.25 sec 405 nm laser pulse (10–30 W/cm^2) was applied. The samples were then immediately illuminated with the imaging lasers again. The number of molecules that recovered was counted and compared with the original number of molecules present at the beginning to give the recovery fraction. The recovery fraction values reported were corrected for non-violet-induced blinking by subtracting the average number of molecules per frame in the 100 frames preceding the application of the 405 nm laser pulse.

Immunofluorescence staining of cellular structures

Immunostaining was performed using BS-C-1 cells (American Type Culture Collection) cultured with Eagle's Minimum Essential Medium fortified with 10% fetal bovine serum, penicillin and streptomycin, and incubated at 37°C with 5% CO_2. Cells were plated in

LabTek 8-well coverglass chambers (154534; Nunc) at ~20,000 cells per well on the day prior to fixation.

The immunostaining procedure for clathrin consisted of: fixation for 20 min with 4% paraformaldehyde (Electron Microscopy Sciences) in PBS; washing with PBS; permeabilization for 2 min with 0.5% Triton X-100 and 3% bovine serum albumin (BSA; Jackson ImmunoResearch Laboratories) in PBS; blocking for 60 min with 0.2% Triton X-100 and 3% BSA in PBS (blocking buffer 1); incubation for 60 min with mouse anti-clathrin heavy chain monoclonal antibody diluted to 2 μg/mL in blocking buffer 1; washing with blocking buffer 1; incubation for 30 min with dye-labeled donkey anti-mouse secondary antibody (~1–2 dyes per antibody) at a concentration of ~2.5 μg/mL in blocking buffer 1; washing with blocking buffer 1; washing with PBS; post-labeling fixation for 10 min with 3% paraformaldehyde and 0.1% glutaraldehyde (Electron Microscopy Sciences) in PBS; and finally washing with PBS.

The immunostaining procedure for microtubules consisted of: fixation for 10 min with 3% paraformaldehyde and 0.1% glutaraldehyde in PBS; washing with PBS; reduction for 5 min with 0.1% sodium borohydride in PBS to reduce background fluorescence; washing with PBS; blocking for 30 min with 3% bovine serum albumin and 0.25% v/v Triton X-100 in PBS (blocking buffer 2); staining for 45 min with primary antibody against tubulin (rat or mouse anti-tubulin) diluted in blocking buffer 2 to a concentration of 10 μg/mL; washing with PBS; incubation for 45 min with secondary antibodies (~1–2 dyes per antibody) at a concentration of ~2.5 μg/mL in blocking buffer 2; washing with PBS; post-labeling fixation for 10 min with 3% paraformaldehyde and 0.1% glutaraldehyde in PBS; and finally washing with PBS.

The procedure for multicolor immunostaining of tubulin, acetylated tubulin, endoplasmic reticulum, and mitochondria was nearly identical to the microtubule immunostaining protocol described above except for the following nucleofection procedures, antibody concentrations, and dye labeling ratios. Prior to seeding, cells had been nucleofected with myc-ATL1 (a gift of Dr. Craig Blackstone[52]) using an Amaxa Nucleofector II (Lonza) with Amaxa Cell Line Nucleofector Kit V (Lonza) approximately 24 hours before fixation. Primary antibodies were used at concentrations of ~10 μg/mL (rat anti-tubulin, goat anti-myc), ~20 μg/mL (mouse antiacetylated tubulin), and ~2 μg/mL (rabbit anti-TOM20) in blocking buffer 2. Secondary antibodies were labeled at a dye-to-protein ratio of ~2.6 Atto 488 dyes per donkey anti-rat antibody, ~1.7 DyLight 750 dyes per donkey anti-mouse antibody, ~1.5 Alexa 647 (or ~1.7 Dyomics 654) dyes per bovine anti-goat antibody, and ~3.1 Cy3B dyes per donkey anti-rabbit antibody.

In vitro assembled microtubules

Microtubules were grown and labeled according to the following protocol. Two prechilled 1 mg tubulin aliquots (T240; Cytoskeleton) were carefully dissolved in a total of 500 μL of a prechilled solution consisting of PEM (100 mM PIPES pH 7.0, 1 mM EGTA, 1 mM $MgCl_2$) with 1 mM GTP (BST06; Cytoskeleton) and 10% glycerol v/v. After centrifugation for 10 min at 18,000 g at 4°C, the supernatant was incubated at 37°C for 20 min to polymerize the microtubules. The microtubules were then stabilized by addition of paclitaxel (TXD01;

Cytoskeleton) to 1 mM and incubation for 5 min at 37°C, and then stored at 25°C. Polymerized microtubules were labeled with dye by incubation of 60 μL of ~4 mg/mL polymerized microtubules with either 0.13 mM Atto488-NHS, 0.16 mM Cy3B-NHS, 0.77 mM Alexa 647-NHS, 0.45 mM Dyomics 654-NHS, or 0.64 mM DyLight 750-NHS for 60 min. Dye-labeled microtubules were purified from free dye by centrifugation through a dense layer consisting of PEM with 60% glycerol (v/v) and 1 mM paclitaxel for 2 hours at 300,000 g. Labeled microtubule pellets were washed carefully and then gently resuspended in 50 μL of buffer consisting of PEM with 1 mM paclitaxel. A set of four single-color labeled microtubule samples was mixed (either Atto 488, Cy3B, Alexa 647, and DyLight 750; or Atto 488, Cy3B, Dyomics 654, and DyLight 750), diluted 1:10 in PEM with 1 mM paclitaxel, and incubated for 10 min in LabTek 8-well chambers which had been cleaned by sonication in 1 M aqueous potassium hydroxide and silanized by incubation with 1% N-(2-aminoethyl)-3-aminopropyl trimethoxysilane (UCT Specialties LLC), 5% acetic acid, and 94% methanol for 20 min to facilitate microtubule adsorption to coverglass. The immobilized microtubules were fixed by incubation for 10 min with 0.5% glutaraldehyde in PEM with 1 mM paclitaxel followed by washing with PEM.

STORM imaging of immunostained cells and *in vitro* microtubules

STORM imaging of immunostained cells was performed using one of five different buffer conditions described in the “Imaging buffers” section. Samples were illuminated with oblique incidence and detected using different excitation sources, dichroic mirrors, and emission filters depending on the fluorophore, as described in the “Fluorescence microscope” section. For 3D STORM imaging, a 1 m cylindrical lens was inserted into the detection path in order to introduce astigmatism such that the images from individual molecules typically appeared elliptical. The *xy* and *z* position of the molecules were determined from the centroid position and the ellipticity of the image, respectively, as previously described[40]. To determine the *z* position of the molecule from the ellipiticity of the single-molecule image, a calibration curve of the change in ellipiticity for different z positions is needed. The calibration curve was determined prior to imaging by recording fluorescence from single immobilized beads (580/605 nm, 200 nm diameter microspheres; Molecular Probes) while scanning the *z*-piezo stage over an 800 nm range (400 nm above and below the central focal plane where the molecule images are circular rather than elliptical).

All STORM movies for blue-, yellow-, and red-absorbing dyes were collected at a frame rate of 61 Hz while those for NIR-absorbing dyes were collected at 33 Hz. An illumination intensity of 1–3 kW/cm^2 was used for these movies. Under this imaging condition, all dye molecules are typically in the fluorescent state initially, but rapidly switch to a dark state. Recording of STORM movies was started once a low density of fluorescent molecules was attained (after ~10–300 sec illumination) such that the images from individual fluorescence molecules were largely not overlapped with each other. All movie durations were 30,000–80,000 frames and were collected using constant illumination at the corresponding excitation wavelength for the dye. For fluorophores that were sensitive to activation with violet light (Table 2), we used continuous-wave 405 nm laser light (0.1–30 W/cm^2,

gradually increased during the movie to illuminate the sample in order to maintain a convenient density of activated molecules.

For multicolor imaging, dyes were imaged sequentially: DyLight 750 first, followed by Alexa 647 (or Dyomics 654), Cy3B, and lastly Atto 488. Filters were switched between data sets for each color. About 70,000 frames were recorded in each color channel before switching to another channel. Simultaneous imaging of differently colored probes is in principle possible by properly separating the fluorescence emissions in the different color channels. However, due to substantial activation of the red and NIR dyes by the blue light used to image Atto 488, the imaging quality may be compromised if all four color ranges were to be imaged simultaneously. For alignment between different color channels, bright-field images of 250 nm Au beads (790128-010; Corpuscular) were taken before each STORM movie and used to register each channel into a common reference frame. We determined that the alignment error was <20 nm, based on control experiments performed with beads that emit in all four spectral bands (data not shown).

STORM image analysis and rendering

STORM movies were analyzed as described previously using custom-written software in IDL and C++[6,40]. Briefly, individual frames were convolved with a zero-sum Gaussian to suppress image noise. Fluorescence peaks corresponding to individual molecules were identified in each frame and fit using least-squares fitting with either a two-dimensional rotating cylindrical or elliptical Gaussian to determine the (x,y) position of each molecule. Maximum-likelihood estimator fitting of fluorophore positions could also be used[53,54]. For 3D imaging, the ellipticity of the Gaussian was used to assign a z coordinate as described previously[40]. Briefly, single-molecule images were fit to an elliptical Gaussian to obtain the centroid position coordinates (x and y) and the Gaussian widths (dx and dy). The z position was calculated from dx and dy using a calibration curve independently determined by scanning bead samples along the z-direction as described in the “Fluorescence microscope” section. Each bead image was also fit to an elliptical Gaussian to obtain the Gaussian widths, dx and dy, and the average dx and dy values from many beads at different z positions were used to create the calibration curve. Molecules that were within a distance of 160 nm (one pixel) in successive frames were linked together and the mean position of the molecule in successive frames was used to report the position of that molecule.

Lateral and axial drift in the sample during acquisition was corrected computationally using image correlation as described previously[6]. Briefly, the STORM movie was segmented into non-overlapping, 2,000–4,000 frame segments, and the STORM image reconstructed from each segment was correlated to the first one in the series to monitor sample drift. This approach relies on maintaining a sufficient density of localizations from each set of frames to ensure the accuracy of the correlation. As mentioned above, STORM movies were taken using 405 nm activation with gradually increasing intensity to maintain this density. However, in the case of imaging a low-copy number structure or imaging a moving sample[20], fiducial markers, such as fluorescent or gold beads, should be used to track sample drift.

Finally, STORM images were rendered with each localization plotted as a Gaussian whose width is weighted by the inverse square root of the number of detected photons for that switching event. Images were filtered to reject molecules that are too dim (<300 photons), too 40 elliptical (*x* and *y* axial ratio >1.5 for 2D images), or that are "on" for >8 consecutive frames. Additional details on data analysis can be found elsewhere[49,55].

Cellular autofluorescence and non-specifically bound antibodies can give background in the STORM images which appears as scattered localizations at low local densities. This background noise was removed in the four-color immunofluorescence images by a local density filter. Specifically, low-density localizations were filtered out by removing a localization if it was surrounded by fewer than 1–3 localizations in the 60 nm × 60 nm region surrounding the localization.

Radial density analysis of clathrin-coated pits

To determine the radial density of localizations for clathrin-coated pits (CCPs), the STORM images of ten CCPs were selected for each dye (Alexa 647, Atto 655, and Cy5.5) and a 40 nm thick *xy* cross-section was taken at the midplane for each CCP. The cross-section images were then merged by aligning the center of mass for each pit to a common point. The localization density was calculated by determining the radial distance of each localization relative to the alignment point. The localizations were then binned and normalized by the area of each radial slice.

Crosstalk analysis

To determine crosstalk between spectral channels (Fig. 4g and Supplementary Fig. 34g), we obtained super-resolution images of *in vitro* assembled microtubules labeled with one of the four probes in each of the four channels. For example, to determine the crosstalk of Alexa 647 into other channels, we imaged microtubules labeled with Alexa 647 in the DyLight 750 channel, followed by the Alexa 647 channel, the Cy3B channel, and lastly the Atto 488 channel, the same imaging sequence as used in our actual imaging experiments. The percent of localizations contributing to the crosstalk was then determined from the STORM image in the DyLight 750, Cy3B, and Atto 488 channels relative to the correct Alexa 647 channel. This procedure was repeated for each of the dyes used in multicolor imaging. We note that in the crosstalk measurements, each dye was imaged for ~40,000 frames in each channel. Imaging for ~40,000 frames in the correct channel (for example imaging Alexa 647 in the red channel) cause partial beaching of the dyes, which could reduce the apparent crosstalk into the bluer channels imaged later in the sequence. However, because our four-color imaging experiments (Fig. 4a, 5, Supplementary Fig. 33a, 35) used exactly the same red-to-blue imaging sequence but with a larger number of frames (~70,000 frames) per channel, which could lead to a larger extent of photobleaching than the crosstalk analysis experiments, we anticipate that the above crosstalk analysis actually overestimates the real crosstalk present in our four-color images.

Supplementary Material

Refer to Web version on PubMed Central for supplementary material.

ACKNOWLEDGEMENTS

The authors thank C. Blackstone (National Institutes of Health) for the myc-ATL1 construct. This work is supported in part by the US National Institutes of Health (to X.Z.). J.C.V. is supported in part by a Burroughs-Wellcome Career Award at the Scientific Interface. K.H.C. acknowledges a National Science Scholarship from the Agency for Science, Technology and Research of Singapore. X.Z. is a Howard Hughes Medical Institute investigator.

REFERENCES

1. Hell SW. Far-field optical nanoscopy. Science. 2007; 316:1153–1158. [PubMed: 17525330]
2. Huang B, Babcock H, Zhuang X. Breaking the diffraction barrier: super-resolution imaging of cells. Cell. 2010; 143:1047–1058. [PubMed: 21168201]
3. Rust MJ, Bates M, Zhuang X. Sub-diffraction-limit imaging by stochastic optical reconstruction microscopy (STORM). Nat. Methods. 2006; 3:793–796. [PubMed: 16896339]
4. Betzig E, et al. Imaging intracellular fluorescent proteins at nanometer resolution. Science. 2006; 313:1642–1645. [PubMed: 16902090]
5. Hess ST, Girirajan TPK, Mason MD. Ultra-high resolution imaging by fluorescence photoactivation localization microscopy. Biophys. J. 2006; 91:4258–4272. [PubMed: 16980368]
6. Bates M, Huang B, Dempsey GT, Zhuang X. Multicolor super-resolution imaging with photo-switchable fluorescent probes. Science. 2007; 317:1749–1753. [PubMed: 17702910]
7. Folling J, et al. Photochromic rhodamines provide nanoscopy with optical sectioning. Angew. Chem. Int. Ed. Engl. 2007; 46:6266–6270. [PubMed: 17640007]
8. Bock H, et al. Two-color far-field fluorescence nanoscopy based on photoswitchable emitters. Appl. Phys. B. 2007; 88:161–165.
9. Conley NR, Biteen JS, Moerner WE. Cy3-Cy5 covalent heterodimers for single-molecule photoswitching. J. Phys. Chem. B. 2008; 112:11878–11880. [PubMed: 18754575]
10. Folling J, et al. Fluorescence nanoscopy by ground-state depletion and single-molecule return. Nat. Methods. 2008; 5:943–945. [PubMed: 18794861]
11. Heilemann M, et al. Subdiffraction-resolution fluorescence imaging with conventional fluorescent probes. Angew. Chem. Int. Ed. Engl. 2008; 47:6172–6176. [PubMed: 18646237]
12. Huang B, Jones SA, Brandenburg B, Zhuang X. Whole-cell 3D STORM reveals interactions between cellular structures with nanometer-scale resolution. Nat. Methods. 2008; 5:1047–1052. [PubMed: 19029906]
13. Flors C, Ravarani CN, Dryden DT. Super-resolution imaging of DNA labelled with intercalating dyes. Chemphyschem. 2009; 10:2201–2204. [PubMed: 19554598]
14. Zhuang XW. Nano-imaging with STORM. Nat. Photonics. 2009; 3:365–367. [PubMed: 20300445]
15. Heilemann M, van de Linde S, Mukherjee A, Sauer M. Super-resolution imaging with small organic fluorophores. Angew. Chem. Int. Ed. Engl. 2009; 48:6903–6908. [PubMed: 19670280]
16. Vogelsang J, Cordes T, Forthmann C, Steinhauer C, Tinnefeld P. Controlling the fluorescence of ordinary oxazine dyes for single-molecule switching and superresolution microscopy. Proc. Natl. Acad. Sci. USA. 2009; 106:8107–8112. [PubMed: 19433792]
17. Belov VN, Wurm CA, Boyarskiy VP, Jakobs S, Hell SW. Rhodamines NN: a novel class of caged fluorescent dyes. Angew. Chem. Int. Ed. Engl. 2010; 49:3520–3523. [PubMed: 20391447]
18. Lee HL, et al. Superresolution imaging of targeted proteins in fixed and living cells using photoactivatable organic fluorophores. J. Am. Chem. Soc. 2010; 132:15099–15101. [PubMed: 20936809]
19. Schwering M, et al. Far-field nanoscopy with reversible chemical reactions. Angew. Chem. Int. Ed. Engl. 2011; 50:2940–2945. [PubMed: 21404374]
20. Jones SA, Shim SH, He J, Zhuang X. Fast, three-dimensional super-resolution imaging of live cells. Nat. Methods. 2011; 8:499–508. [PubMed: 21552254]
21. Baddeley D, et al. 4D super-resolution microscopy with conventional fluorophores and single wavelength excitation in optically thick cells and tissues. PLoS One. 2011; 6:e20645. [PubMed: 21655189]

22. Fernandez-Suarez M, Ting AY. Fluorescent probes for super-resolution imaging in living cells. Nat. Rev. Mol. Cell. Biol. 2008; 9:929–943. [PubMed: 19002208]
23. Patterson G, Davidson M, Manley S, Lippincott-Schwartz J. Superresolution imaging using single-molecule localization. Annu. Rev. Phys. Chem. 2010; 61:345–367. [PubMed: 20055680]
24. Hoyer P, Staudt T, Engelhardt J, Hell SW. Quantum dot blueing and blinking enables fluorescence nanoscopy. Nano Lett. 2011; 11:245–250. [PubMed: 21128678]
25. Habuchi S, et al. Reversible single-molecule photoswitching in the GFP-like fluorescent protein Dronpa. Proc. Natl. Acad. Sci., USA. 2005; 102:9511–9516. [PubMed: 15972810]
26. Brakemann T, et al. A reversibly photoswitchable GFP-like protein with fluorescence excitation decoupled from switching. Nat. Biotechnol. 2011
27. Grotjohann T, et al. Diffraction-unlimited all-optical imaging and writing with a photochromic GFP. Nature. 2011
28. Patterson GH, Lippincott-Schwartz J. A photoactivatable GFP for selective photolabeling of proteins and cells. Science. 2002; 297:1873–1877. [PubMed: 12228718]
29. Subach FV, et al. Photoactivatable mCherry for high-resolution two-color fluorescence microscopy. Nat. Methods. 2009; 6:153–159. [PubMed: 19169259]
30. Chudakov DM, et al. Photoswitchable cyan fluorescent protein for protein tracking. Nat. Biotechnol. 2004; 22:1435–1439. [PubMed: 15502815]
31. Wiedenmann J, et al. EosFP, a fluorescent marker protein with UV-inducible green-to-red fluorescence conversion. Proc. Natl. Acad. Sci., USA. 2004; 101:15905–15910. [PubMed: 15505211]
32. McKinney SA, Murphy CS, Hazelwood KL, Davidson MW, Looger LL. A bright and photostable photoconvertible fluorescent protein. Nat. Methods. 2009; 6:131–133. [PubMed: 19169260]
33. Gurskaya NG, et al. Engineering of a monomeric green-to-red photoactivatable fluorescent protein induced by blue light. Nat. Biotechnol. 2006; 24:461–465. [PubMed: 16550175]
34. Sharonov A, Hochstrasser RM. Wide-field subdiffraction imaging by accumulated binding of diffusing probes. Proc. Natl. Acad. Sci., USA. 2006; 103:18911–18916. [PubMed: 17142314]
35. Bates M, Huang B, Zhuang X. Super-resolution microscopy by nanoscale localization of photo-switchable fluorescent probes. Curr. Opin. Chem. Biol. 2008; 12:505–514. [PubMed: 18809508]
36. Thompson RE, Larson DR, Webb WW. Precise nanometer localization analysis for individual fluorescent probes. Biophys. J. 2002; 82:2775–2783. [PubMed: 11964263]
37. Yildiz A, et al. Myosin V walks hand-over-hand: Single fluorophore imaging with 1.5 nm localization. Science. 2003; 300:2061–2065. [PubMed: 12791999]
38. Shroff H, Galbraith CG, Galbraith JA, Betzig E. Live-cell photoactivated localization microscopy of nanoscale adhesion dynamics. Nat. Methods. 2008; 5:417–423. [PubMed: 18408726]
39. van de Linde S, et al. Direct stochastic optical reconstruction microscopy with standard fluorescent probes. Nat. Protoc. 2011; 6:991–1009. [PubMed: 21720313]
40. Huang B, Wang W, Bates M, Zhuang X. Three-dimensional super-resolution imaging by stochastic optical reconstruction microscopy. Science. 2008; 319:810–813. [PubMed: 18174397]
41. Dani A, Huang B, Bergan J, Dulac C, Zhuang X. Superresolution imaging of chemical synapses in the brain. Neuron. 2010; 68:843–856. [PubMed: 21144999]
42. Bates M, Blosser TR, Zhuang X. Short-range spectroscopic ruler based on a single-molecule optical switch. Phys. Rev. Lett. 2005; 94:108101. [PubMed: 15783528]
43. Heilemann M, Margeat E, Kasper R, Sauer M, Tinnefeld P. Carbocyanine dyes as efficient reversible single-molecule optical switch. J. Am. Chem. Soc. 2005; 127:3801–3806. [PubMed: 15771514]
44. Dempsey GT, et al. Photoswitching mechanism of cyanine dyes. J. Am. Chem. Soc. 2009; 131:18192–18193. [PubMed: 19961226]
45. van de Linde S, et al. Photoinduced formation of reversible dye radicals and their impact on super-resolution imaging. Photochem. Photobiol. Sci. 2011; 10:499–506. [PubMed: 21152594]
46. Steinhauer C, Forthmann C, Vogelsang J, Tinnefeld P. Superresolution microscopy on the basis of engineered dark states. J. Am. Chem. Soc. 2008; 130:16840–16841. [PubMed: 19053449]

47. Kottke T, Van de Linde S, Sauer M, Kakorin S, Heilemann M. Identification of the Product of Photoswitching of an Oxazine Fluorophore Using Fourier Transform Infrared Difference Spectroscopy. J. Phys. Chem. Lett. 2010; 1:3156–3159.

48. Testa I, et al. Multicolor fluorescence nanoscopy in fixed and living cells by exciting conventional fluorophores with a single wavelength. Biophys. J. 2010; 99:2686–2694. [PubMed: 20959110]

49. Dempsey, GT.; Wang, W.; Zhuang, X. Handbook of Single-molecule Biophysics. Hinterdorfer, P.; van Oijen, AM., editors. Springer Science and Business Media; 2009. p. 95-127.

50. Riddles PW, Blakeley RL, Zerner B. Reassessment of Ellman's reagent. Methods Enzymol. 1983; 91:49–60. [PubMed: 6855597]

51. Rasnik I, McKinney SA, Ha T. Nonblinking and longlasting single-molecule fluorescence imaging. Nat. Mathods. 2006; 3:891–893.

52. Zhu PP, et al. Cellular localization, oligomerization, and membrane association of the hereditary spastic paraplegia 3A (SPG3A) protein atlastin. J. Biol. Chem. 2003; 278:49063–49071. [PubMed: 14506257]

53. Mortensen KI, Churchman LS, Spudich JA, Flyvbjerg H. Optimized localization analysis for single-molecule tracking and super-resolution microscopy. Nat. Methods. 2010; 7:377–381. [PubMed: 20364147]

54. Laurence TA, Chromy BA. Efficient maximum likelihood estimator fitting of histograms. Nat. Methods. 2010; 7:338–339. [PubMed: 20431544]

55. Bates, M.; Jones, S.; Zhuang, X. Imaging: A Laboratory Manual. Yuste, R., editor. Cold Spring Harbor Laboratory Press; 2011. p. 547-576.

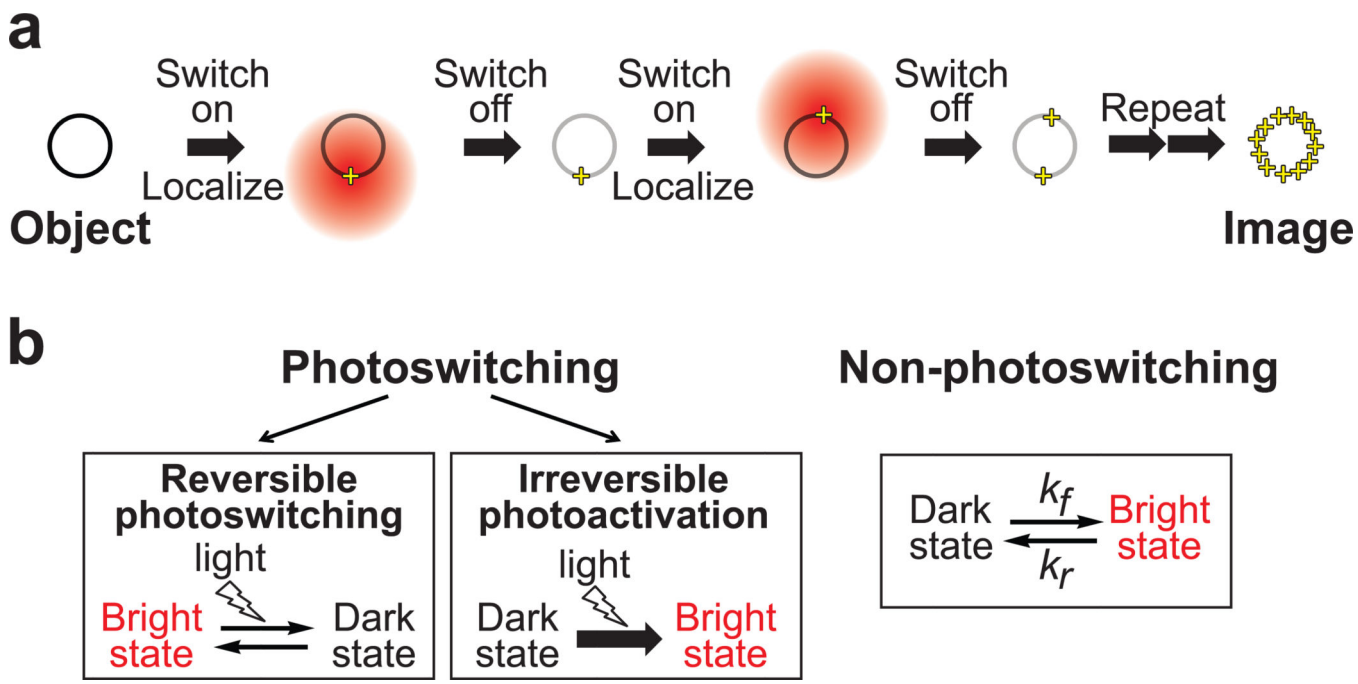

Figure 1. Principle of single-molecule-localization-based super-resolution imaging and modes of switching used for this imaging method

(**a**) A structure (here a ring-like object) smaller than the diffraction-limited resolution is densely labeled with switchable fluorophores. When the fluorophores are imaged simultaneously, the spatial features of the structure are obscured by the overlapping fluorescence images of each molecule. However, the positions of individual molecules may be determined with high precision when the molecules are activated and imaged sequentially (fluorescent image indicated as a red circle whose center position is marked as a yellow '+'). By repeatedly activating and localizing different molecules labeling the structure, the sub-diffraction-limited spatial features can be resolved. (**b**) This principle can be performed by utilizing photoswitching or non-photoswitching modes. The first mode further includes reversibly switchable or irreversibly activatable fluorophores. The non-photoswitching mode can be achieved, for example, through reversible binding of fluorescently labeled ligands or chemical quenching of fluorescence.

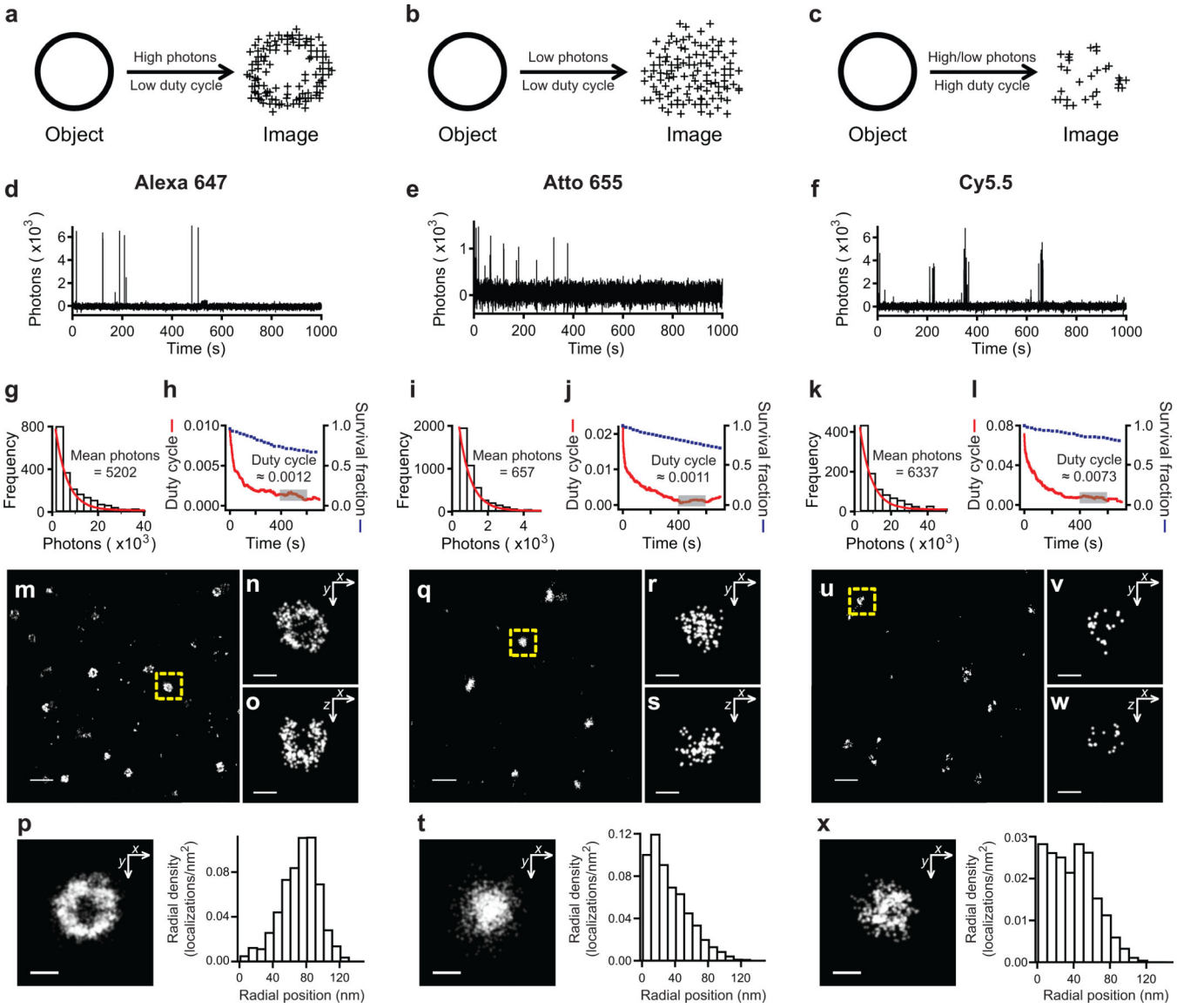

Figure 2. Quantitative probe characterization for STORM imaging

(**a**–**c**) The effect of number of detected photons per on-switching event and the on/off duty cycle (fraction of time in the on state) on STORM image quality for an example structure (a ring-like object). (**a**) A fluorophore with high photon number and low duty cycle produces a hollow, ring-like image with high localization precision and sufficient density. (**b**) A fluorophore with low photon number and low duty cycle maintains a large number of localizations, but suffers reduced localization accuracy, obscuring the ring-like structure. (**c**) A fluorophore with high on/off duty cycle requires reduction in the density of fluorescent probes to allow single-molecule localization, which in turn reduces the number of localizations and adversely affects the overall resolution. Single-molecule fluorescence time traces measured in the presence of βME and an oxygen scavenging system, as shown for three red-absorbing dyes (**d**) Alexa 647, (**e**) Atto 655, and (**f**) Cy5.5. Each of these dyes represents one of the scenarios described in (**a–c**). From these traces, the number of detected

photons was determined for each switching event and a histogram was constructed from many events from hundreds of molecules (**g**,**i**,**k**). The indicated mean value was derived from the single exponential fit of the distribution (red curve). The on/off duty cycle value was calculated for each dye and plotted versus time (red curve; **h**,**j**,**l**) to show how each value begins high when most molecules are in the fluorescent state and reaches a quasi-equilibrium at a later time. The reported values are the average duty cycle measured between 400–600 sec (gray box). The fraction of molecules that survived photobleaching was plotted together with the duty cycle (blue squares). Images of clathrin-coated pits (CCPs) in 3D using the three dyes. (**m–p**) Alexa 647, (**q–t**) Atto 655, and (**u–x**) Cy5.5. The large fields of view shown in (**m,q,u**) are 2D projection images. The images of the CCPs indicated by the yellow dashed boxes are magnified and their *xy* cross-sections (**n**,**r**,**v**) and *xz* cross-sections (**o**,**s**,**w**) are shown. The composite *xy* cross-sections for ten CCPs aligned to their respective centers of mass are shown along with the radial density distributions of localizations derived from the composite *xy* cross-sections (**p**,**t**,**x**). Scale bars are 500 nm for (**m**,**q**,**u**) and 100 nm for (**n–p**, **r–t**, **v–x**).

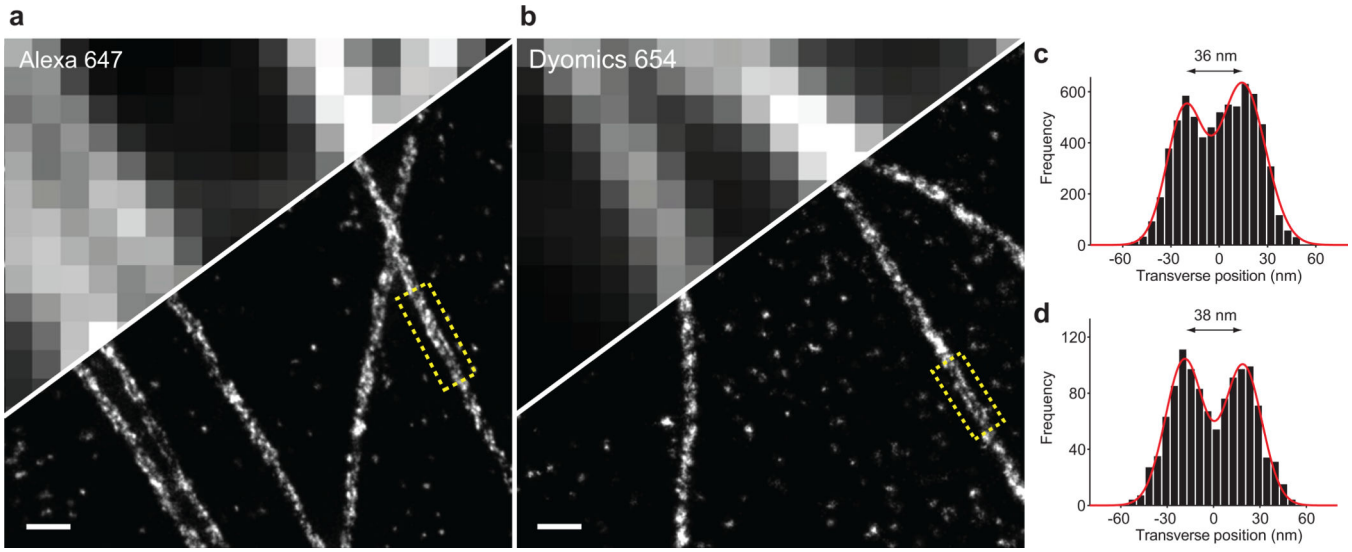

Figure 3. Alexa 647 and Dyomics 654 resolve the hollow structure of immunostained microtubules

(**a–b**) STORM images of microtubules immunostained with Alexa 647 (**a**) and Dyomics 654 (**b**) and the partially overlaid conventional fluorescence images in the upper left corner of each image. (**c–d**) The transverse profiles of localizations corresponding to the yellowboxed regions in (**a–b**) illustrate the hollow cylindrical structure of the filament with a pronounced dip in the center (top panel corresponds to (**a**) and the bottom panel corresponds to (**b**)). Fitting of the profile by two Gaussian functions (red lines) gave the expected distances between the two peaks. Scale bars: 250 nm.

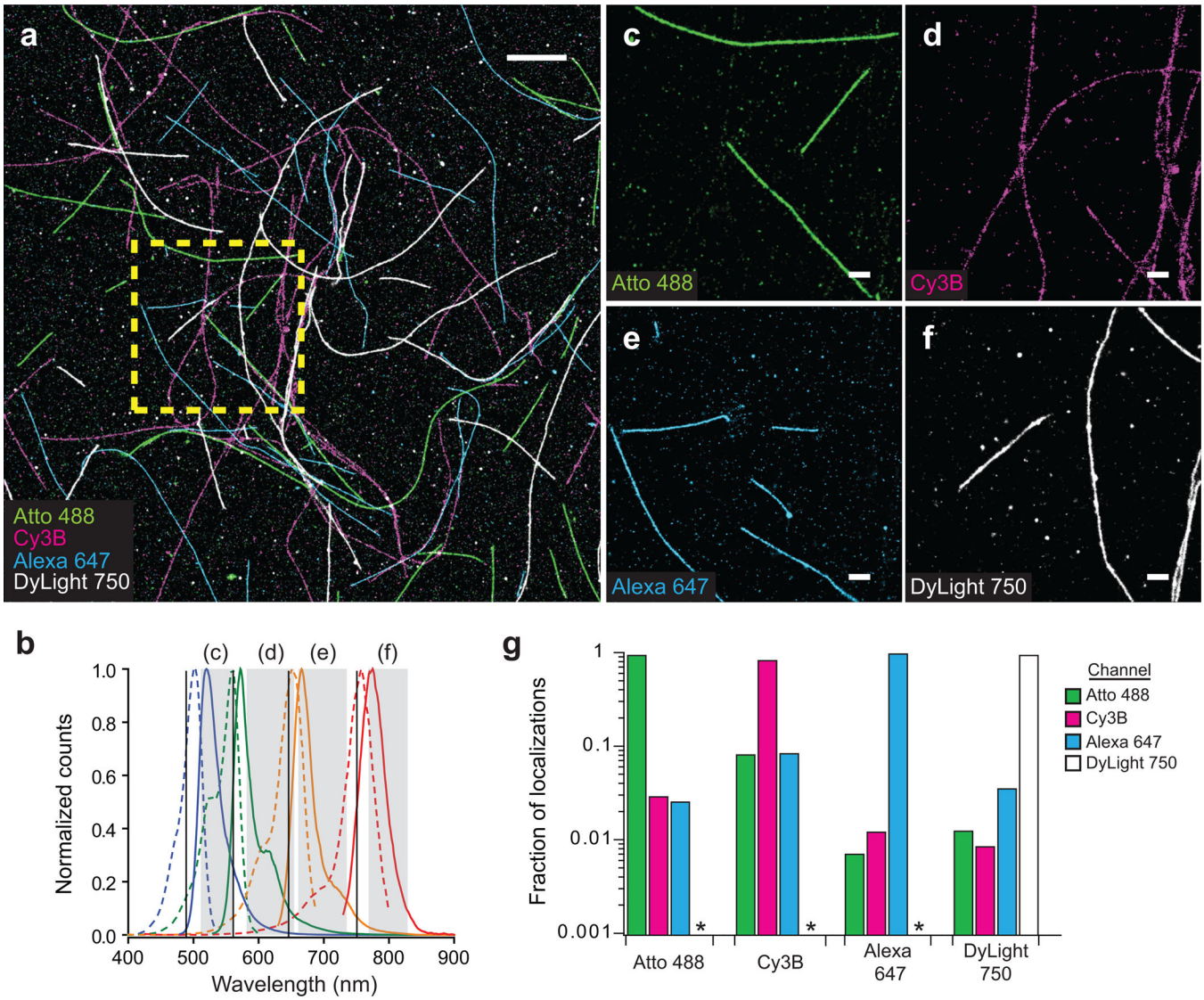

Figure 4. Four-color STORM imaging of *in vitro* assembled microtubule filaments and crosstalk analysis

(**a**) Four-color STORM image of *in vitro* assembled microtubules labeled with each of the four dyes, Atto 488 (green), Cy3B (magenta), Alexa 647 (cyan), and DyLight 750 (white). (**b**) Spectral separation of the four dyes, with the black vertical lines representing the excitation wavelength used and the gray regions highlighting the emission filter range for each of the dyes in (**c–f**). (**c–f**) Individual STORM images in each of the spectral regions for the boxed region in (**a**). (**g**) The crosstalk between channels measured from control microtubule samples (see **Methods** section for details). The asterisks indicate that the crosstalk was undetectable in those channels. Scale bars: 2 μm for (**a**) and 500 nm for (**c–f**).

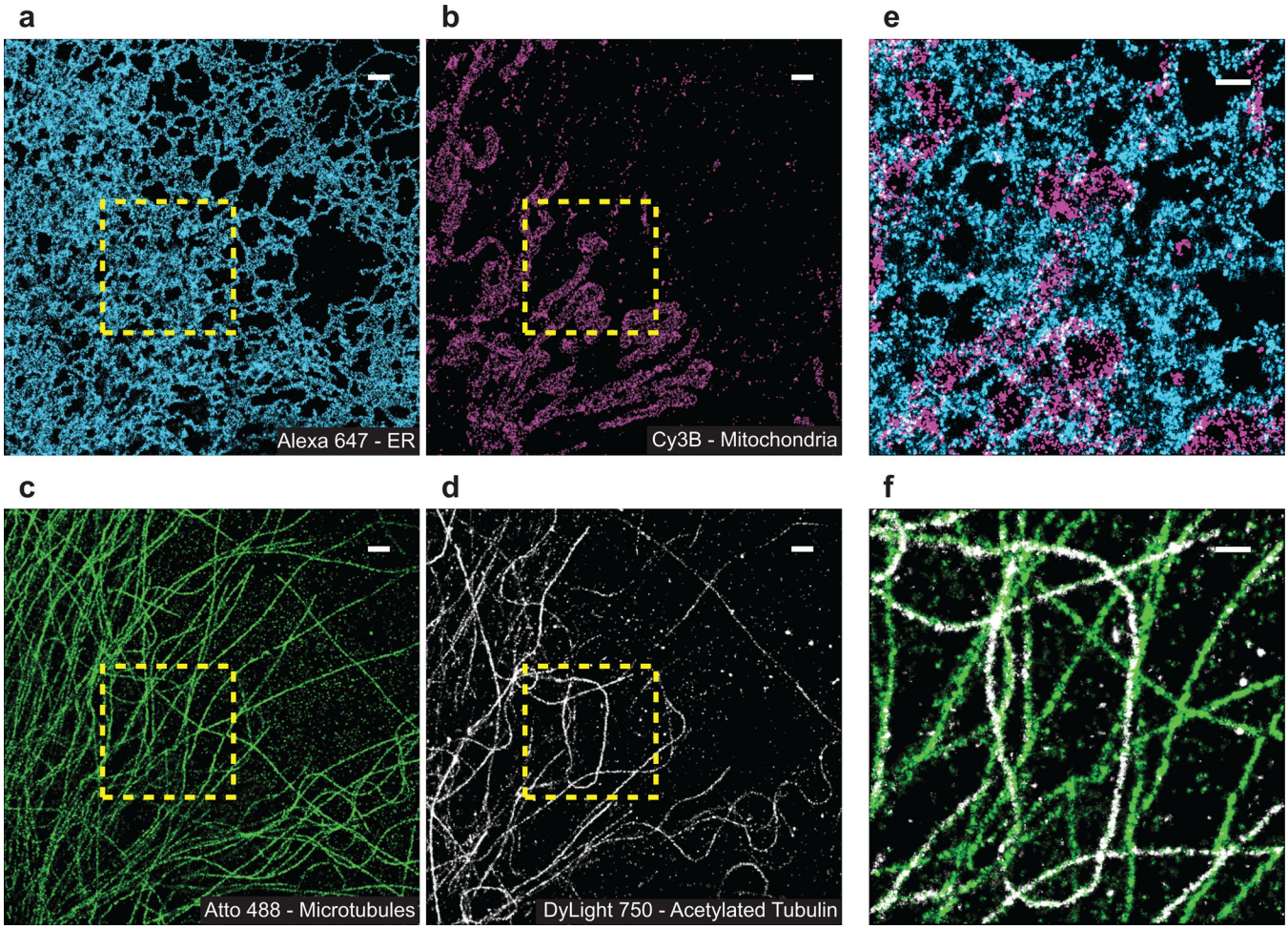

Figure 5. Four-color STORM imaging of cellular structures

(**a–d**) Individual channels of a four-color image of Atto 488-labeled microtubules (green), Cy3B-labeled mitochondria (magenta), Alexa 647-labeled ER (cyan), and DyLight 750-labeled acetylated tubulin (white) within a single fixed cell. The dashed yellow box in each panel corresponds to the same region in the image. (**e**) Zoom-in of the Cy3B and Alexa 647 channels of the yellow-boxed region in (**a–d**) showing extensive contact between mitochondria and the ER. (**f**) Zoom-in of the Atto 488 and DyLight 750 channels of the same region show overlap of acetylated tubulin with a subset of microtubule filaments. Scale bars: 1 μm for (**a–d**) and 500 nm for (**e–f**).

Table 1

Summary of switching properties of the 26 dyes tested in this study

Tabulated dye switching properties include: number of detected photons per switching event; equilibrium on-off duty cycle taken between 400 and 600 sec; the survival fraction after illumination for 400 sec; and the number of switching cycles. The dye switching properties are reported in the presence of GLOX and 10 mM MEA as well as GLOX and 140 mM βME. Also included are additional dye properties: excitation and emission peak wavelengths from the dye spectra; extinction coefficients from the dye manufacturers; and quantum yields from either the dye manufacturer when known or from the McNamara 2007 fluorophore data tables. The excitation wavelength, dichroic mirrors, and emission filters used for characterization and imaging for each spectral range, respectively, are as follows: 488 nm, T495LP (Chroma), and ET535/50m (Chroma) for blue-absorbing dyes; 561 nm, Di01-R561 (Semrock), and FF01-617/73-25 (Semrock) for yellow-absorbing dyes; 647 nm, Z660DCXRU (Chroma), and ET700/75m (Chroma) for red-absorbing dyes; 752 nm, Q770DCXR (Chroma), and HQ800/60m (Chroma) for NIR-absorbing dyes.

Dye		Excitation Maximum (nm)	Emission Maximum (nm)	Extinction (M^{-1} cm^{-1})	Quantum Yield	Detected Photons Per Cycle		Equilibrium Duty Cycle		Survival Fraction (400 s)		# Switching Cycles (Mean)	
						MEA	βME	MEA	βME	MEA	βME	MEA	βME
Blue-absorbing	Atto 488	501	523	90,000	0.8	1,341	1,110	0.00065	0.0022	0.98	0.99	11	49
	Alexa 488	495	519	71,000	0.92	1,193	427	0.00055	0.0017	0.94	1	16	139
	Atto 520	516	538	110,000	0.9	1,231	868	0.0015	0.00061	0.92	0.86	9	17
	Fluorescein	494	518	70,000	0.79	1,493	776	0.00032	0.00034	0.51	0.83	4	15
	FITC	494	518	70,000	0.8	639	1,086	0.00041	0.00031	0.75	0.9	17	16
	Cy2	489	506	150,000	0.12	6,241	4,583	0.00012	0.00045	0.12	0.19	0.4	0.7
Yellow-absorbing	Cy3B	559	570	130,000	0.67	1,365	2,057	0.0003	0.0004	1	0.89	8	5
	Alexa 568	578	603	91,300	0.69	2,826	1,686	0.00058	0.0027	0.58	0.99	7	52
	TAMRA	546	575	90,430	0.2	4,884	2,025	0.0017	0.0049	0.85	0.99	10	59
	Cy3	550	570	150,000	0.15	11,022	8,158	0.0001	0.0003	0.17	0.55	0.5	1.6
	Cy3.5	581	596	150,000	0.15	4,968	8,028	0.0017	0.0005	0.89	0.61	5.7	3.3
	Atto 565	563	592	120,000	0.9	19,714	13,294	0.00058	0.00037	0.17	0.26	4	5
Red-absorbing	Alexa 647	650	665	239,000	0.33	3,823	5,202	0.0005	0.0012	0.83	0.73	14	26
	Cy5	649	670	250,000	0.28	4,254	5,873	0.0004	0.0007	0.75	0.83	10	17
	Atto 647	645	669	120,000	0.2	1,526	944	0.0021	0.0016	0.46	0.84	10	24
	Atto 647N	644	669	150,000	0.65	3,254	4,433	0.0012	0.0035	0.24	0.65	9	39
	Dyomics 654	654	675	220,000	–	3,653	3,014	0.0011	0.0018	0.79	0.64	20	19
	Atto 655	663	684	125,000	0.3	1,105	657	0.0006	0.0011	0.65	0.78	17	22

Dye		Excitation Maximum (nm)	Emission Maximum (nm)	Extinction (M^{-1} cm^{-1})	Quantum Yield	Detected Photons Per Cycle		Equilibrium Duty Cycle		Survival Fraction (400 s)		# Switching Cycles (Mean)	
						MEA	βME	MEA	βME	MEA	βME	MEA	βME
	Atto 680	680	700	125,000	0.3	1,656	987	0.0019	0.0024	0.65	0.91	8	27
	Cy5.5	675	694	250,000	0.28	5,831	6,337	0.0069	0.0073	0.87	0.85	16	25
NIR-absorbing	DyLight 750	752	778	220,000	–	712	749	0.0006	0.0002	0.55	0.58	5	6
	Cy7	747	776	200,000	0.28	852	997	0.0003	0.0004	0.48	0.49	5	2.6
	Alexa 750	749	775	240,000	0.12	437	703	0.00006	0.0001	0.36	0.68	1.5	6
	Atto 740	740	764	120,000	0.1	779	463	0.00047	0.0014	0.31	0.96	3	14
	Alexa 790	785	810	260,000	–	591	740	0.00049	0.0014	0.54	0.62	5	2.7
	IRDye 800 CW	778	794	240,000	–	2,753	2,540	0.0018	0.038	0.6	1	3	127

– Quantum yield values not available from dye manufacturer or McNamara data tables.

Table 2

Sensitivity to violet photoactivation for the 26 dyes tested in this study

The fraction of single fluorescent molecules that activate after a 0.25 sec pulse of 405 nm excitation light (10–30 W/cm^2) relative to the total initial population was measured for each dye.

Dye		Sensitivity to activation by violet light
Blue-absorbing	Atto 488	+
	Alexa 488	+
	Atto 520	+
	fluorescein	−
	FITC	−
	Cy2	−
Yellow-absorbing	Cy3B	+
	Alexa 568	+
	TAMRA	−
	Cy3	−
	Cy3.5	+
	Atto 565	+
Red-absorbing	Alexa 647	++
	Cy5	++
	Atto 647	+
	Atto 647N	+
	Dyomics 654	++
	Atto 655	+
	Atto 680	+
	Cy5.5	++
NIR-absorbing	Dylight 750	++
	Cy7	++
	Alexa 750	++
	Atto 740	+
	Alexa 790	++
	IRDye 800CW	++

Dyes were assigned a “−”, “+”, or “++” if <3%, 3–25%, or >25% were reactivated, respectively.

Table 3

Evaluation of the effect of buffer composition on the switching properties for the 26 dyes tested in this study

Cells were immunostained against microtubules for each of the dyes. Photoswitching was tested under each of the listed buffer conditions: No GLOX or thiol, Thiol only, GLOX only, and GLOX + thiol. The thiol used was MEA.

Dye		Buffer Condition			
		No GLOX or thiol	Thiol only	GLOX only	GLOX + thiol
Blue-absorbing	Atto 488	+	+	++	++
	Alexa 488	+	+	++	++
	Atto 520	+	+	++	++
	fluorescein	−	+	+	+
	FITC	−	+	+	+
	Cy2	−	−	−	−
Yellow-absorbing	Cy3B	+	+	++	++
	Alexa 568	−	−	+	+
	TAMRA	−	−	−	+
	Cy3	−	−	+	+
	Cy3.5	−	−	+	+
	Atto 565	−	−	+	+
Red-absorbing	Alexa 647	−	+	−	++
	Cy5	−	+	−	++
	Atto 647	+	+	+	+
	Atto 647N	+	−	−	+
	Dyomics 654	−	+	−	++
	Atto 655	+	+	+	++
	Atto 680	+	+	++	++
	Cy5.5	−	−	−	+
NIR-absorbing	DyLight 750	−	+	−	++
	Cy7	−	+	−	++
	Alexa 750	−	+	−	+

Dye		Buffer Condition			
		No GLOX or thiol	Thiol only	GLOX only	GLOX + thiol
	Atto 740	−	+	+	+
	Alexa 790	−	+	−	+
	IRDye 800CW	−	−	−	−

Dyes were assigned a “−”, “+”, or “++” if rapid bleaching (no image), low to moderate photoswitching (low to moderate quality image), or robust photoswitching (high quality image) was observed, respectively. While lower image quality (+) was observed for Atto 647N and Alexa 750 in the GLOX + thiol condition, reasonable image quality (++) was observed for these two dyes when βME was used instead of MEA.